Numerical experiments in idealized glacier topographies

Case study of the impact of the mesh resolution on the prediction of the grounding line position

Ruben ESPELETA BOLIVAR

[1]Institut des geosciences de l'environnement

May 24th, 2023

Content

Institut des géosciences de l'environnement

Definition

Glaciers can be defined as a mass of ice that accumulates from snow and flows slowly downwards

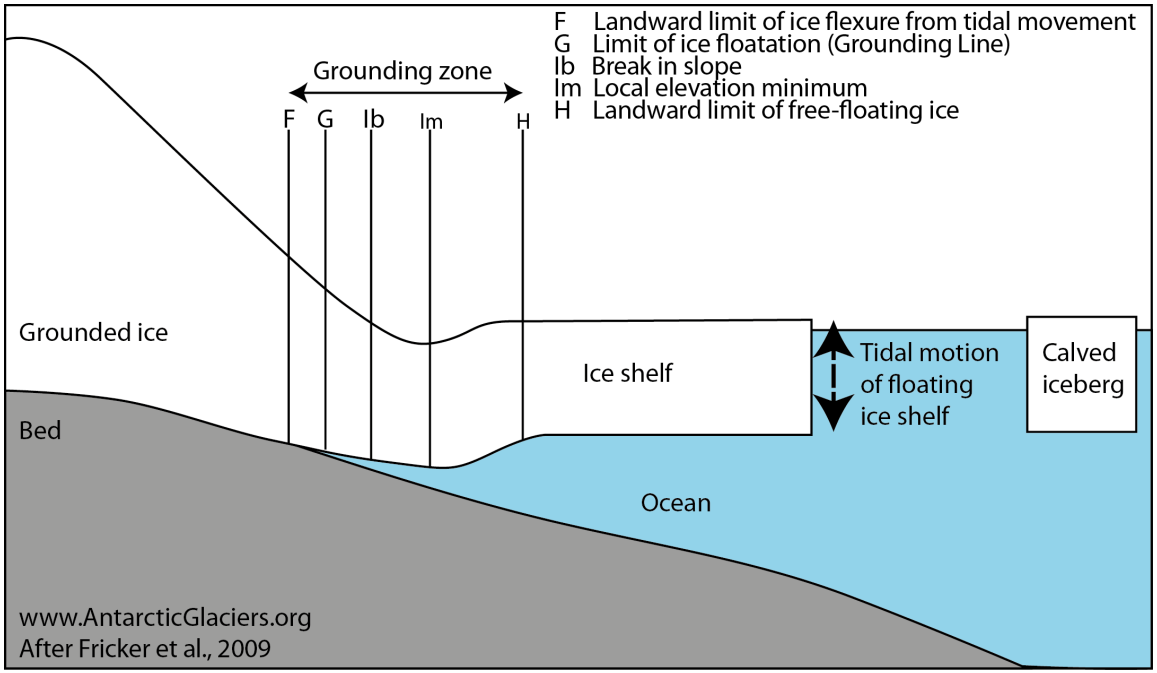

Figure: Schema of a tributary glacier where we can observe the different parts denoting the grounding zone (Fricker et al., 2009). Adapted from AntarticGlaciers.org

Importance of understanding the dynamics of glaciers

- The rate of present-day sea-level rise has increased in recent decades and it is expected to continue increasing in coming decades and centuries (Clark et al., 2015).
- Morlighem et al. (2017) and Haywood et al. (2011) mentioned that if all the ice were to melt completely, the sea level would rise by an estimated of 65m.
- The Unites Nations states that around 40% of the world's population lives in coastal regions, within 100km of the coastline (Barbier, 2015; Montgomery, 2007).
- The land area that is less than 10m above sea level is just 2% of the world's total land area, yet it is home to 10% of the world's population and 13% of the world's urban population (Nevermann et al., 2023).

IGE
Institut des géosciences de l'environnement

Incompressibility condition

Ice can be considered an incompressible viscous fluid:

$$\frac{\delta u}{\delta x} + \frac{\delta v}{\delta y} + \frac{\delta w}{\delta z} = 0; \tag{1}$$

The deviatoric normal stress in the x-direction is:

$$\sigma'_{xx} = \sigma_{xx} - P; \tag{2}$$

Where P is the mean normal stress:

$$P = -\frac{1}{3}(\sigma_{xx} + \sigma_{YY} + \sigma_{ZZ}) \tag{3}$$

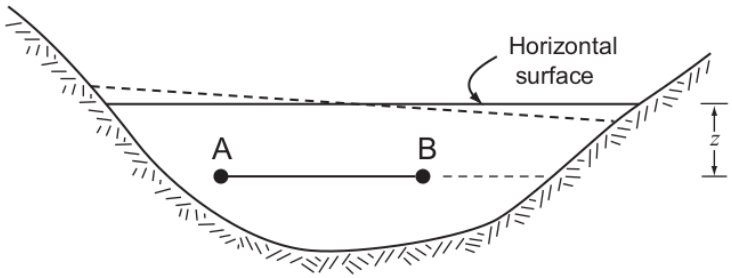

Figure: Sketch to illustrate non-hydrostatic pressure. Adapted from Hooke (2019).

Governing equations I

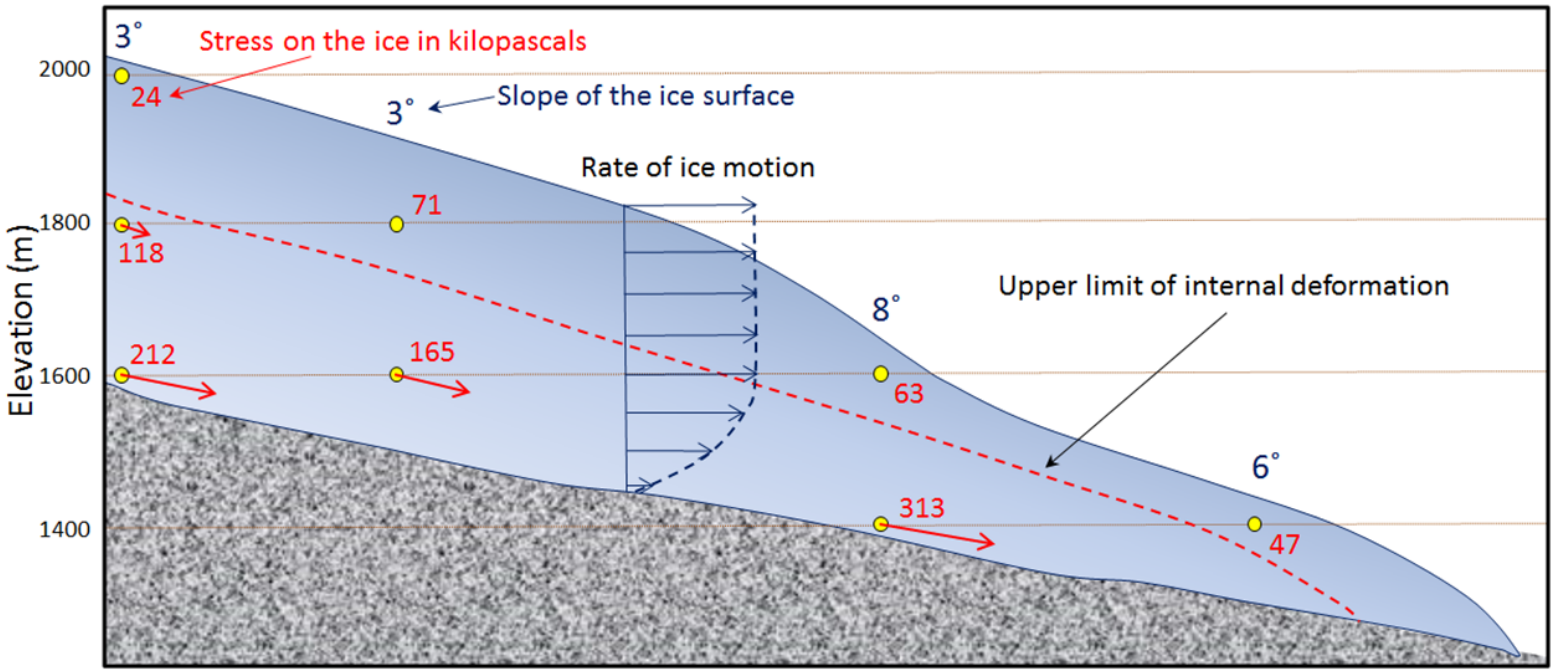

Figure: Stress within a valley glacier (red numbers) and the ice velocity (blue arrows). Figure adapted from Earle (2015)

Governing equations II

The plastic lower ice of the glacier can flow like a very viscous fluid. The incompressibility condition leads to:

$$\nabla u = 0 \tag{4}$$

For ice flow, the acceleration term can be neglected in the Navier-Stokes equations (Hutter, 1982). Therefore:

$$-\nabla p + \nabla(\eta(\nabla u + (\nabla u)^T)) + \rho g = 0; \tag{5}$$

Where η is the viscosity and g is the gravity. Letting σ denote the stress tensor and pressure p is the mean normal stress denoted previously, and the strain rate tensor ϵ_e, related by:

$$\sigma = 2\eta\epsilon_e - pI = \eta(\nabla u + (\nabla u)^T) - pI; \tag{6}$$

Where I is the identity tensor. Together, these two last mathematical equations are called the full-stokes model.

The flow law

The most commonly used flow law for ice is Glen's flow law, named after John W. Glen upon whose experiments it is based Glen (1958). This equation was originally written in the form:

$$\dot{\epsilon_e} = (\frac{\sigma_e}{B})^n; \tag{7}$$

where B is a viscosity parameter that increases as the ice becomes stiffer, and n is an empirically determined constant. Most studies have found that n=3,. An alternative form of the flow law that is commonly used, and that can be used, is:

$$\dot{\epsilon_e} = A{\sigma_e}^n \tag{8}$$

A is called the rate factor. B is normally given in Mpa $\text{yr}^{\frac{1}{n}}$ while A is in MPa^{-n} yr^{-1} or MPa^{-n} s^{-1}.

Boundary conditions and time evolution I

- Ice in contact with the bedrock: Weertman sliding law (Weertman, 1974):

$$u_b = C{\tau_b}^m; \tag{9}$$

- The ice surface is assumed stress free $\sigma.n = 0$ and ice base at z_s and z_b behave as free surfaces according to:

$$\frac{\delta z_i}{\delta t} + u_i \frac{\delta z_i}{\delta x} + v_i \frac{\delta z_i}{\delta y} = w_i + a_i; \tag{10}$$

where a_i is the accumulation ($a_i > 0$) or ablation ($a_i < 0$) in meter ice equivalent per year, and i = surface or base, respectively.

- By vertical integration of the incompressibility condition, w can be eliminated:

$$\frac{\delta H}{\delta t} + \frac{\delta H\bar{u}}{\delta x} + \frac{\delta H\bar{v}}{\delta y} = a_s - a_b;$$

Where $\bar{u}$ and $\bar{v}$ are the vertically integrated horizontal velocities.

Boundary conditions and time evolution II

- For the ice-ocean interface, as soon as the seawater pressure p_w at the ice base z_b is larger than the normal stress exerted by the ice at the bed, the ice is assumed to float. At the ice-ocean interface, the tangential friction is neglected and:

$$\sigma n = -p_w n; \tag{12}$$

where:

$$p_w(z) = -\rho_w g z; z < 0; \tag{13}$$

and $\sigma n = 0$ above sea level ($z > 0$).

Shallow shelf approximation

The conservation of momentum simplifies to:

$$\nabla_h.(2\bar{\eta}(\dot{\epsilon_h}I)) = \rho g H \nabla_h z_s; \tag{14}$$

Where the subscript h represents the components in the x-y plane and $\bar{\eta}$ the vertically integrated viscosity. The effective strain rate simplifies to:

$$\dot{\epsilon_h} = \sqrt{\frac{\delta u}{\delta x}^2 + \frac{\delta v}{\delta y}^2 + \frac{\delta u}{\delta x}\frac{\delta v}{\delta y} + \frac{1}{4}(\frac{\delta u}{\delta y} + \frac{\delta v}{\delta y})^2}; \tag{15}$$

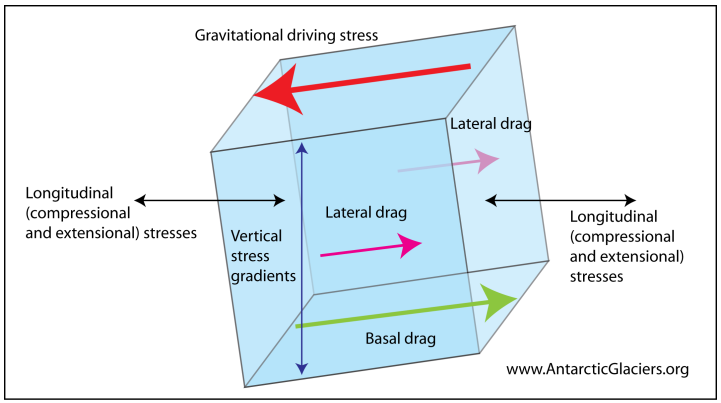

Figure: Driving and basal stresses on a block of ice. Adapted from AntarticGlaciers.org

Grounding line dynamics and stability

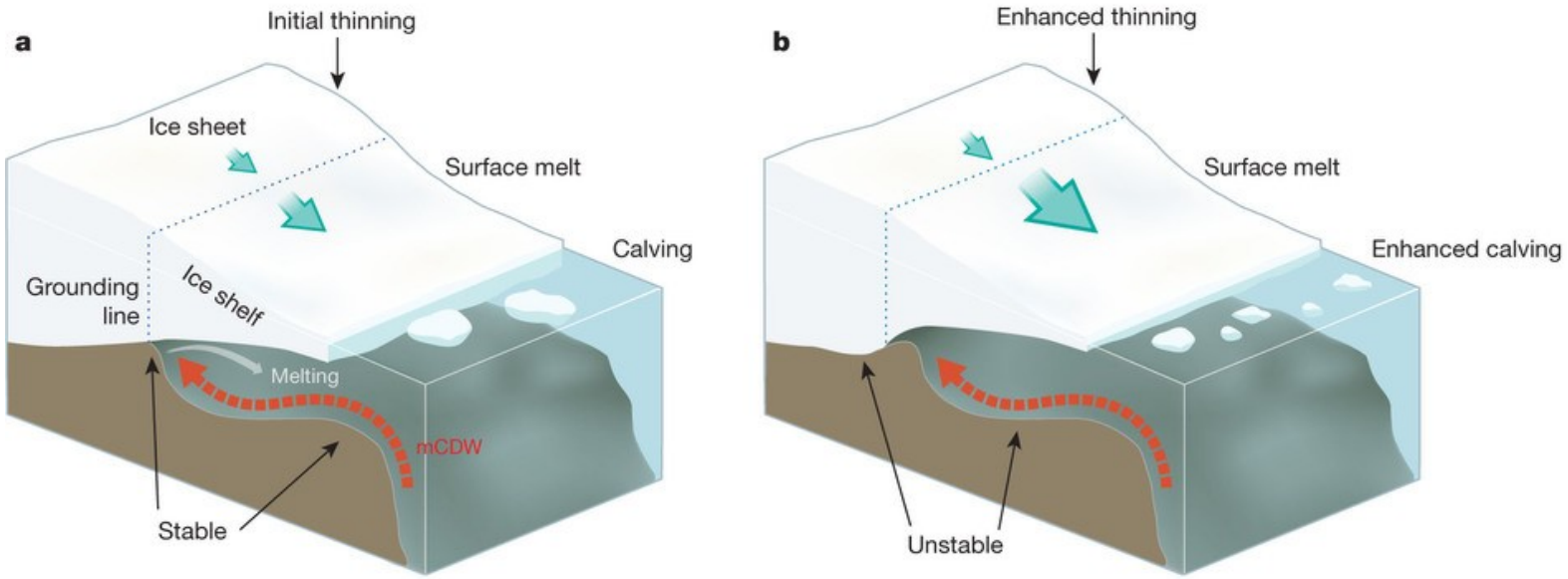

Figure: Schematic representation of the marine ice sheet instability with an initial stable grounding line position (left hand side) and unstable grounding line position after the incursion of warm circumpolar deep water below the ice shelf. Adapted from Hanna et al. (2013).

Process of modelling

The physical phenomena that impacts the dynamics of the glaciers can be represented using mathematical models that implement partial differential equations, which can then be discretized to be solved using numerical methods.

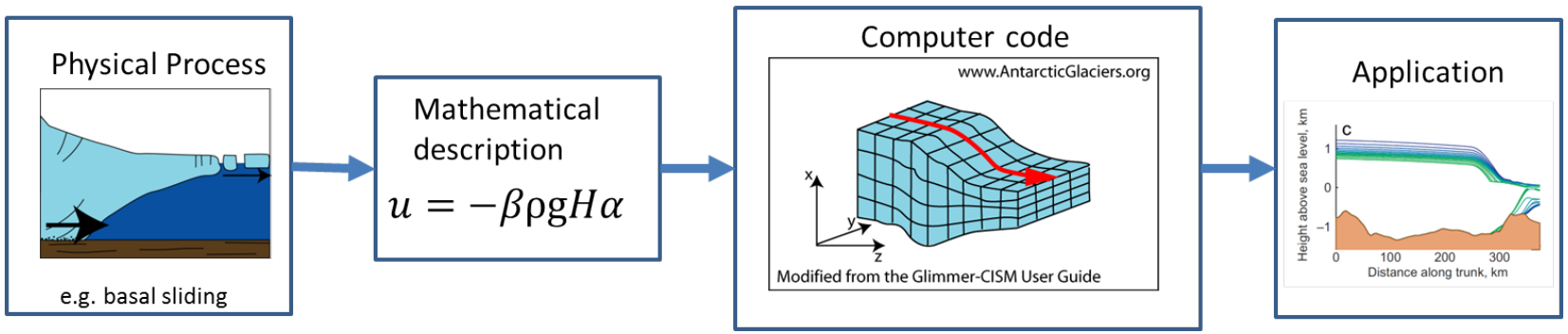

Figure: Process of modelling, starting with a physical phenomena which can be represented mathematically in a physical model than can then be discretized to solve numerically. Adapted from AntarticGlaciers.org

Elmer/Ice finite element method

- Open source finite element code, mainly developed in Finland.
- The ice sheet/ice flow model Elmer/Ice is based on Elmer and includes developments related to glaciological problems. It includes a large number of dedicated solvers and users functions.
- Elmer/Ice solves the Stokes equations and it includes solvers for the approximations of the Stokes equations, namely shallow shelf and shallow ice approximations.

Numerical parameters

Table: Physical parameters

Variable	Description	Units
$g = 9.81$	Gravitational acceleration	ms^{-2}
$a_s = 0.3$	Surface mass balance (SMB)	ma^{-1}
$a_b = 0$	Basal mass balance (BMB)	ma^{-1}
$\rho i = 917$	Ice density	kg m^{-3}
$\rho w = 1028$	Sea water density	kg m^{-3}
$A = 2.9377 \text{x} 10^{-9}$	Ice rate factor	$KPa^{-3}a^{-1}$
$n = 3$	Flow law stress exponent	Dimensionless
$C = 0.001$	basal slipperiness	$ma^{-1}KPa^{-3}$
$m = 3$	Sliding law stress exponent	Dimensionless
$s2a = 31556926$	Seconds in a year	s

Numerical variables, external forcings and initial condition

- The numerical resolution will be the variable parameter, varying from 10km, 5km, 2km, and 1km.
- The external forces acting will be gravity, as well as the ice friction and the basal stress.
- The initial condition will be a topography with no ice, namely h_0=0m.
- The CFL condition will be necessary to verify the stability of the model. It is needed that:

$$C = \frac{u\Delta t}{\Delta x} < C_{max}; \tag{16}$$

where, C is the Courant number, u is the velocity, Δt is the time step, Δx is the horizontal resolution. $C_{max} = 1$ is a safe approximation.

Cone domain I

Systems are proposed in the context of the CalvingMIP inter-comparison project (https://github.com/JRowanJordan/CalvingMIP). The idealised experimental domain comprise a simple, symmetrically circular domain. This first idealized model consists of a circular bedrock configuration (Figure 7) given by:

$$\theta = arctan2(y, x); \tag{17}$$

$$I = r - cos(2\theta)\frac{r}{2} \tag{18}$$

$$Bed_0 = Bc - (Bc - BI)\frac{|x^2 + y^2|}{r^2}; \tag{19}$$

Where r=800x10^3m, Bc=0.9 x 10^3m, and BI=-2 x 10^3m.

Cone domain II

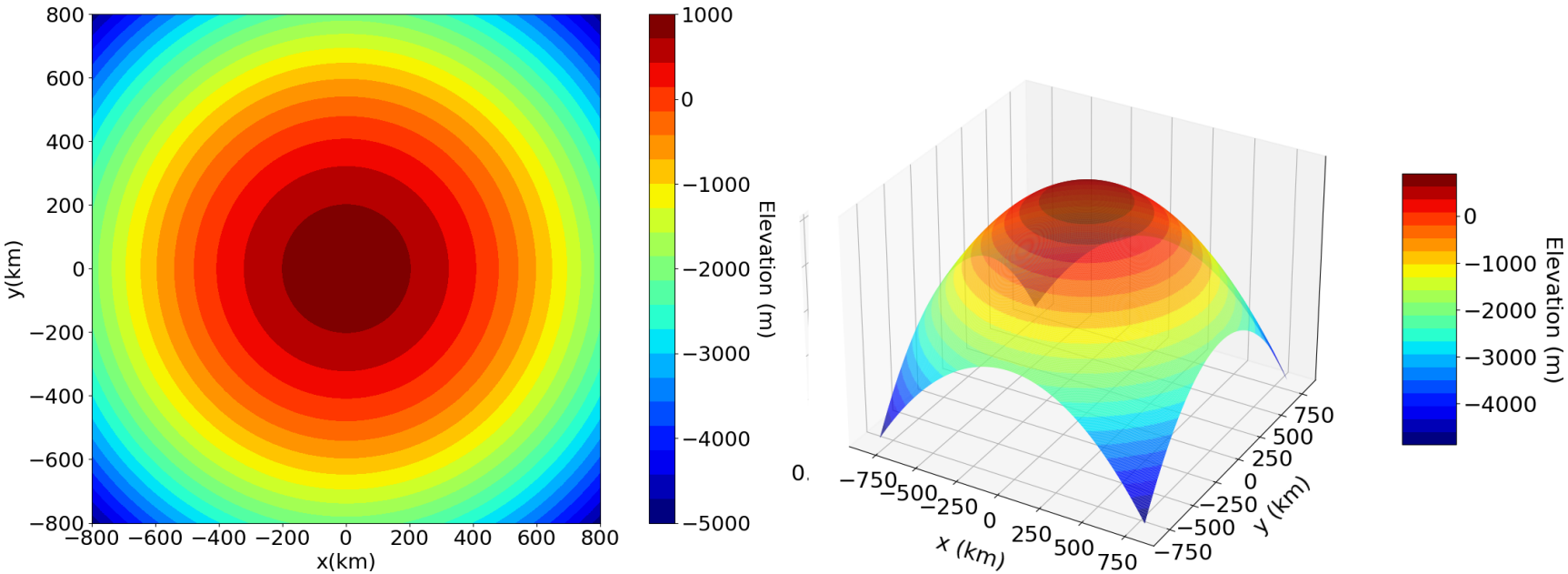

Figure: Circular bedrock topography. On the left side top view and on the right side, lateral view.

Cone domain III

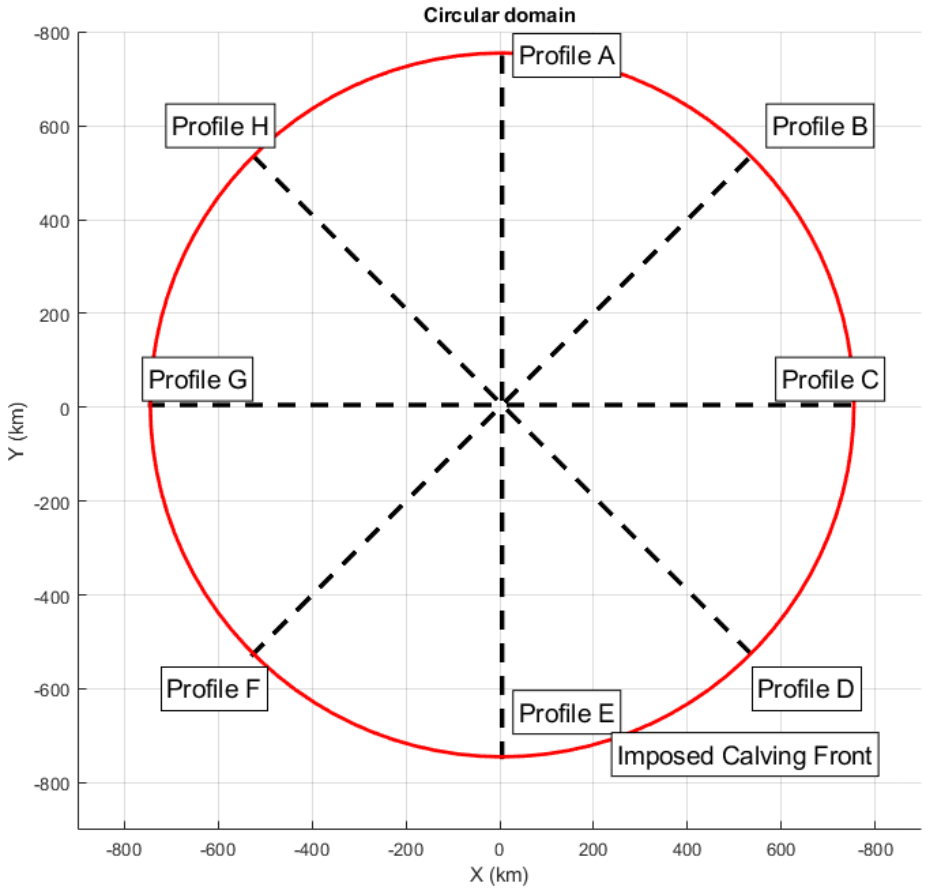

Figure: Circular domain experimental profiles as well as the initial imposed calving front position. Adapted from CalvingMIP inter-comparison project.

Thule domain I

The Thule bedrock configuration is shown in Figure 9 and is given by:

$$\theta = arctan2(y, x); \tag{20}$$

$$I = r - cos(2\theta)\frac{r}{2}; \tag{21}$$

$$Bed_0 = Bc - (Bc - BI)\frac{|x^2 + y^2}{r^2}; \tag{22}$$

$$Bed = Bacos(3\pi\frac{\sqrt[2]{x^2 + y^2}}{I}) + Bed_0; \tag{23}$$

With r=800 x $10^3 m$, Bc=0,9 x $10^3 m$, BI=-2 x $10^3 m$, and Ba=1.1 x $10^3 m$.

Thule domain II

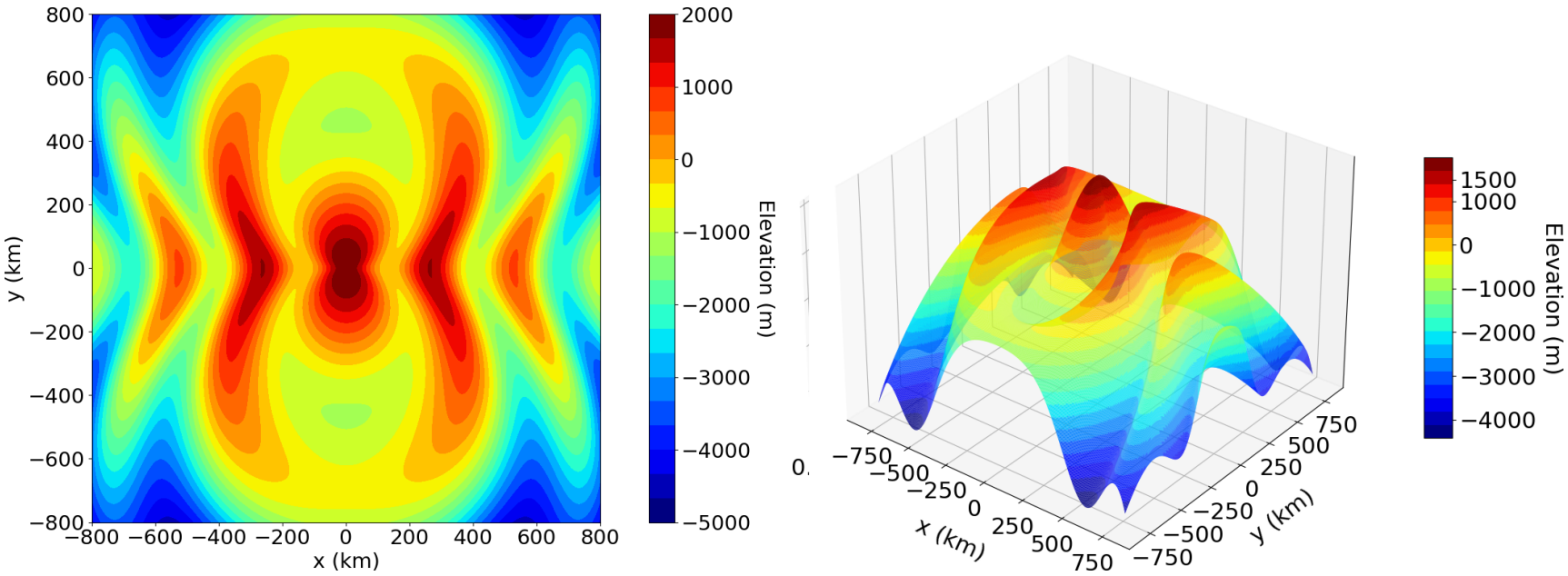

Figure: Thule bedrock topography 3D. On the left side the top view, and on the right side a lateral view.

Thule domain III

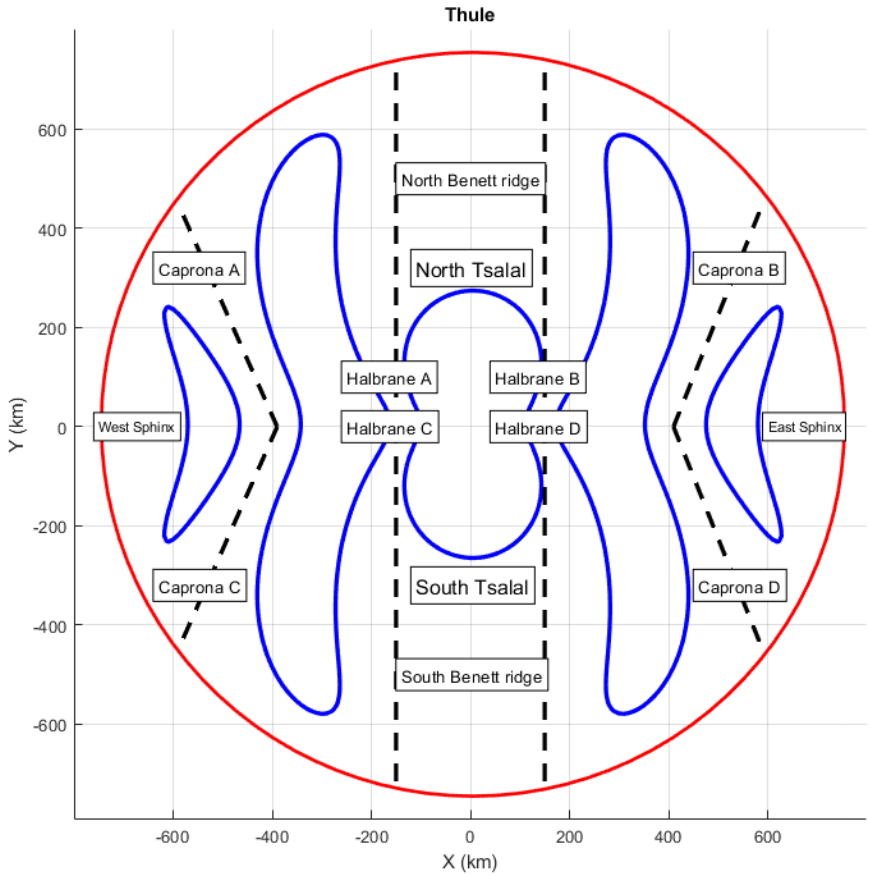

Figure: Thule domain experimental profiles as well as the initial imposed calving front position. Adapted from CalvinMIP inter-comparison project.

Results:Cone domain I

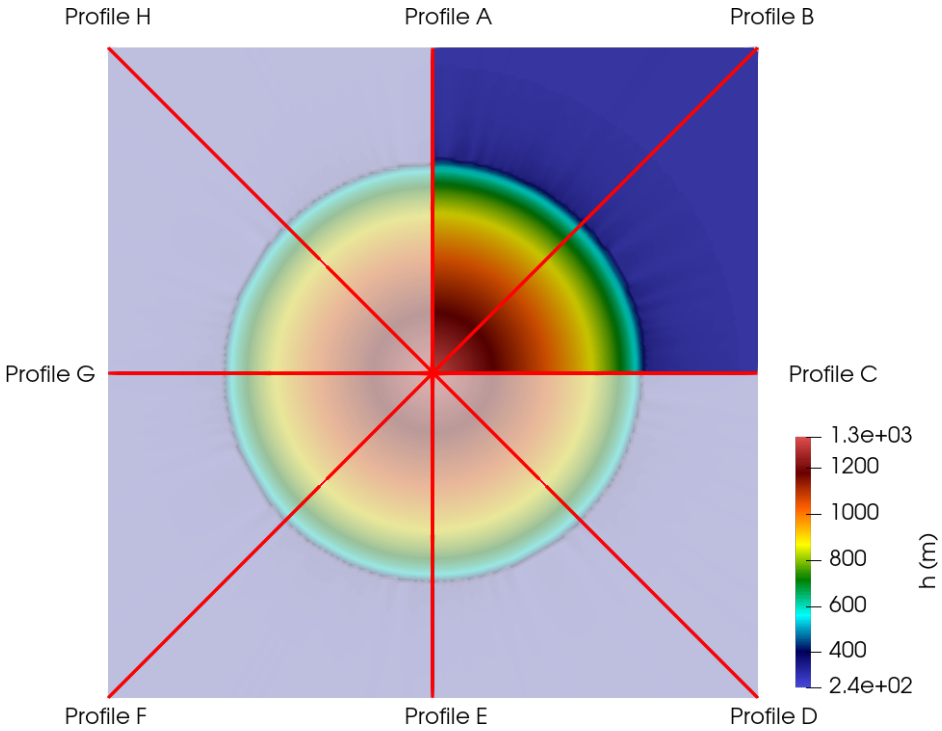

(a) Profiles for Cone circular domain

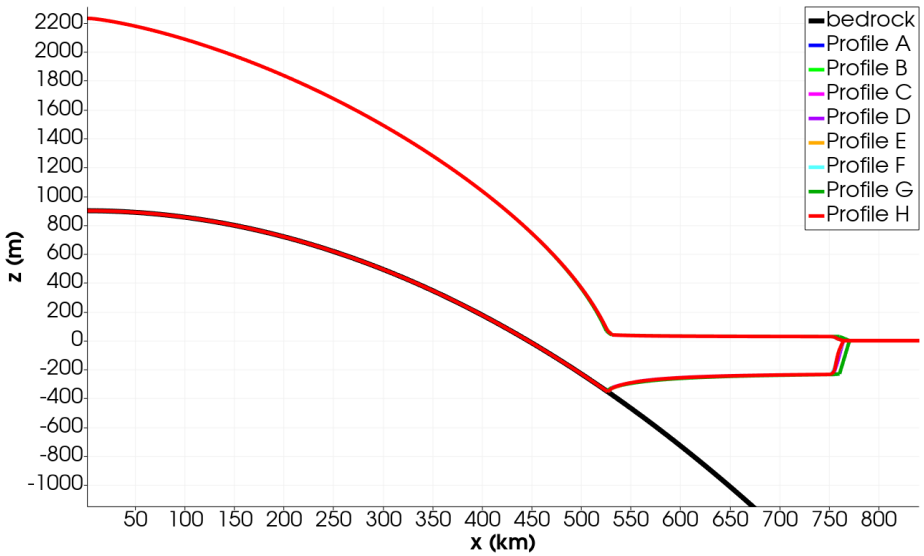

(b) Ice thickess per profile

Figure: Schematic representation of the circular domain ice sheet showing the ice thickness results along the profiles proposed.

Results:Cone domain II

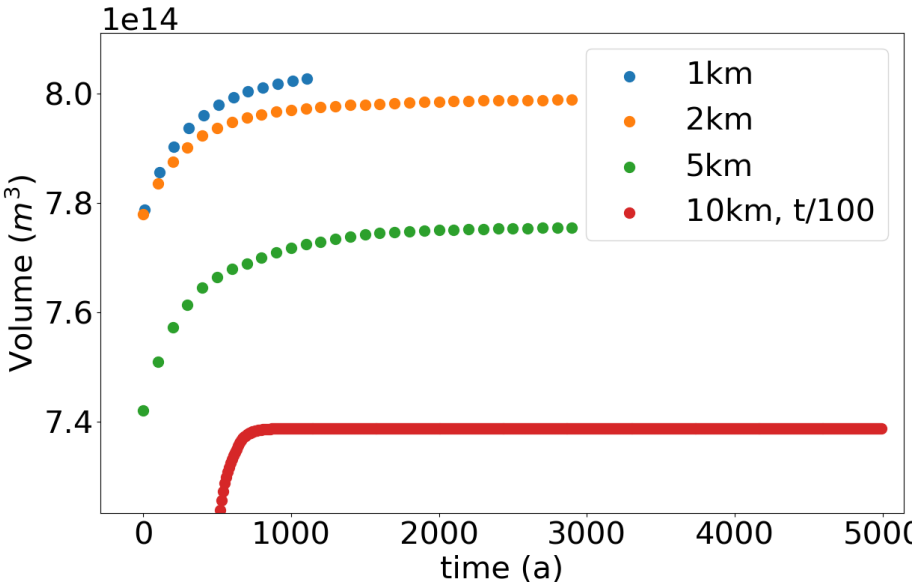

(a) Volume variation in time.

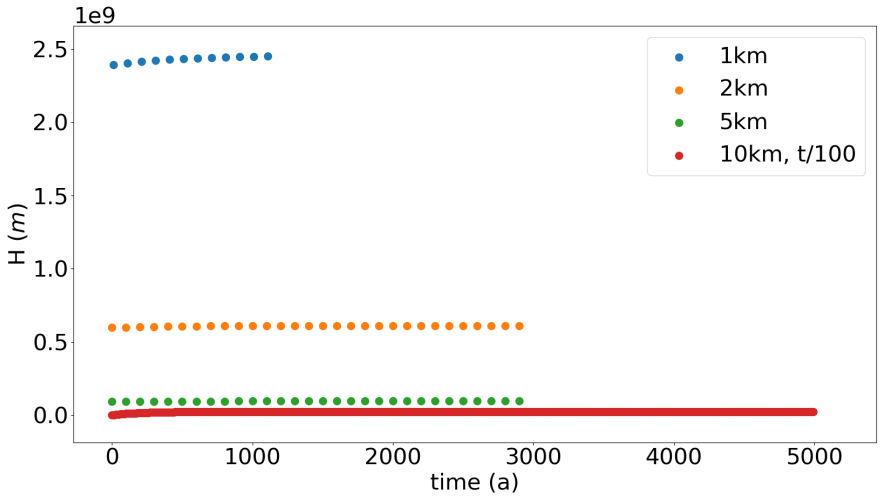

(b) Ice thickess variation in time.

Figure: Volume and thickness variation in time for the cone domain experiment.

Results:Cone domain III

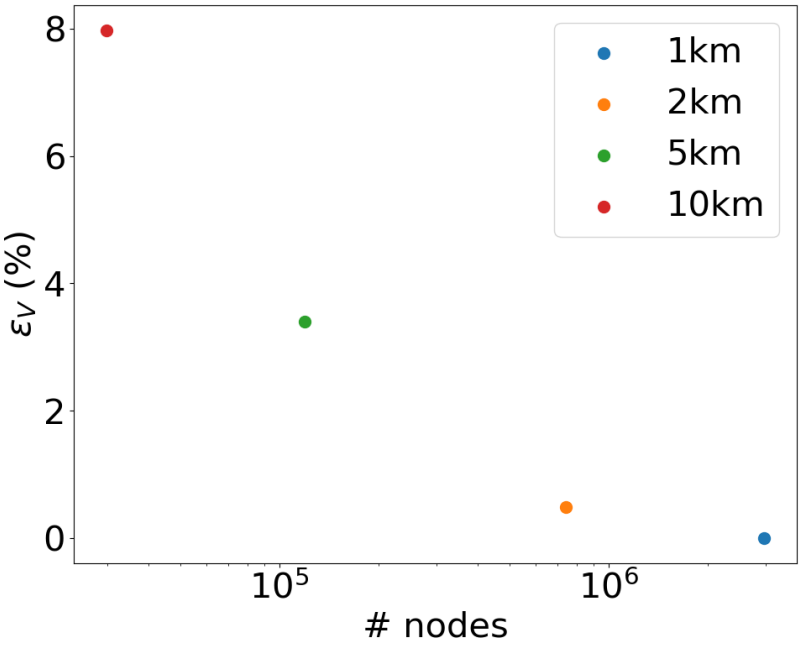

(a) Volume relative variation as a function of the number of nodes.

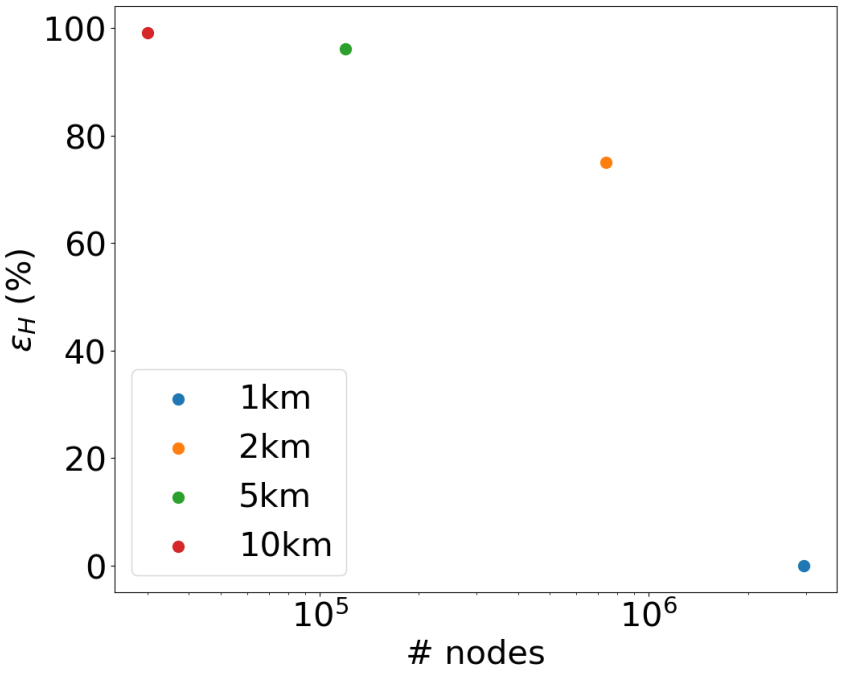

(b) Ice thickness error as a function of the number of nodes.

Figure: Ice thickess and volume variation with respect to the number of nodes for the Cone circular domain experiment.

Results:Cone domain IV

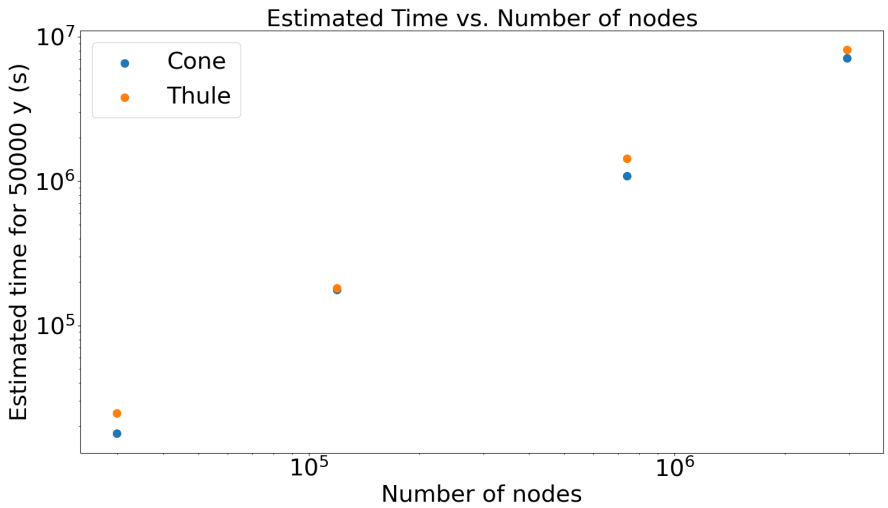

(a) Time for 32 processors used.

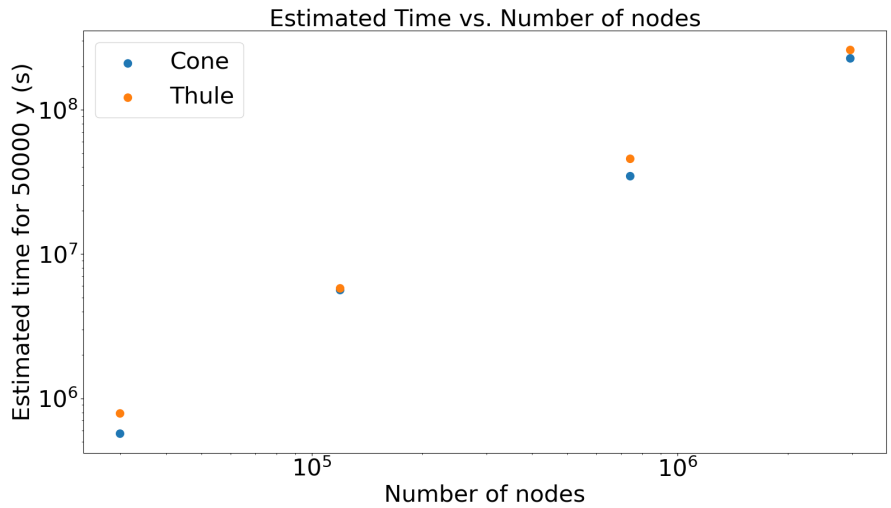

(b) Time for 1 processor.

Figure: Simulation time as a function of the number of nodes for each resolution mesh.

Results:Cone domain V

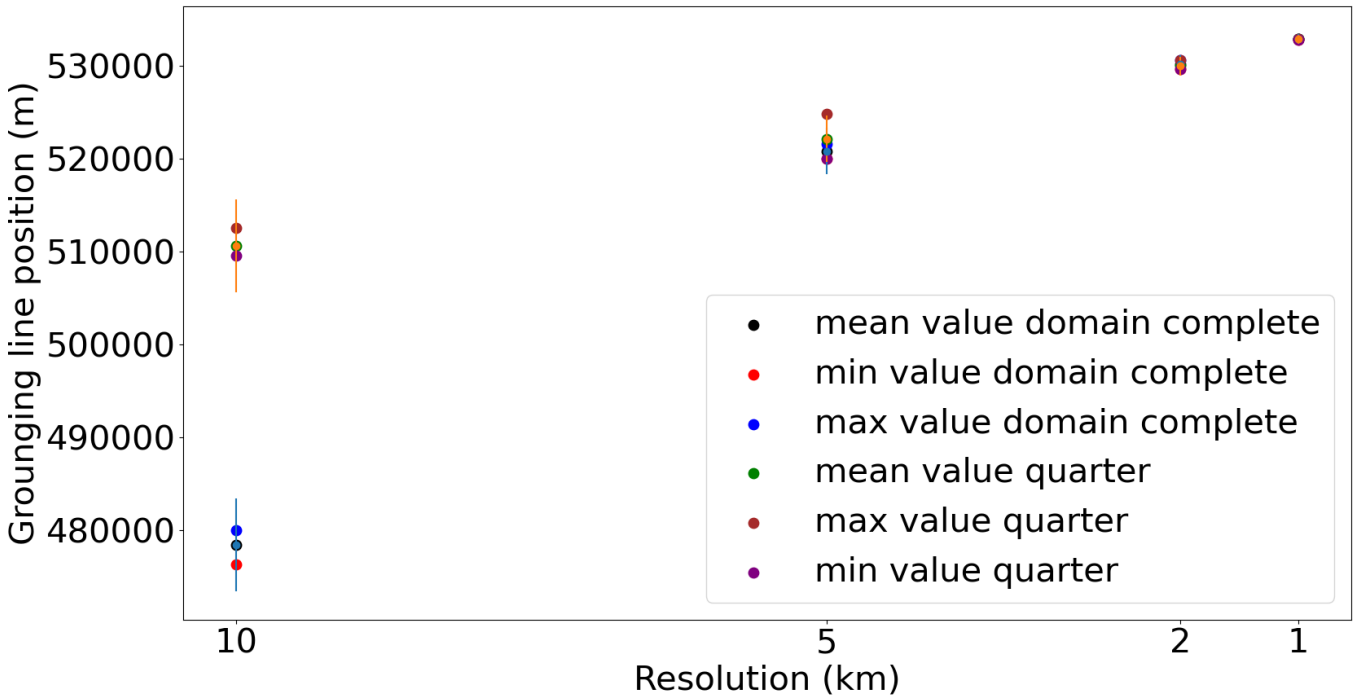

Figure: Grounding line positions as a function of the resolution for quarter and complete circular cone domain.

Results: Thule domain I

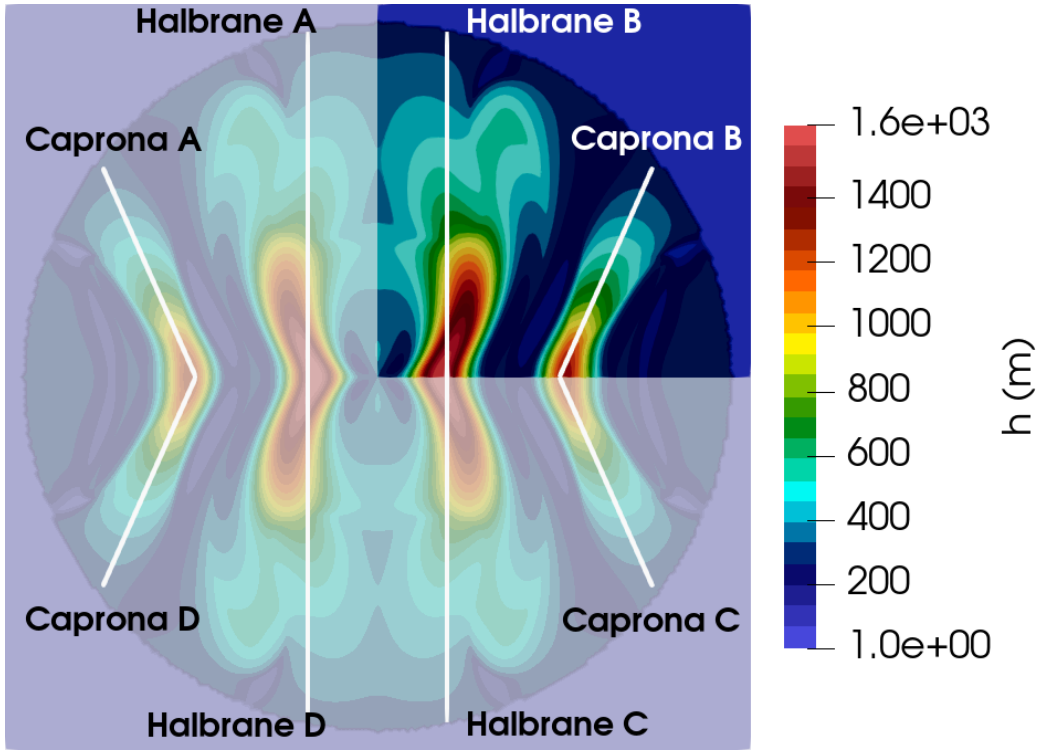

Figure: Profiles for the thule domain

Results: Thule domain II

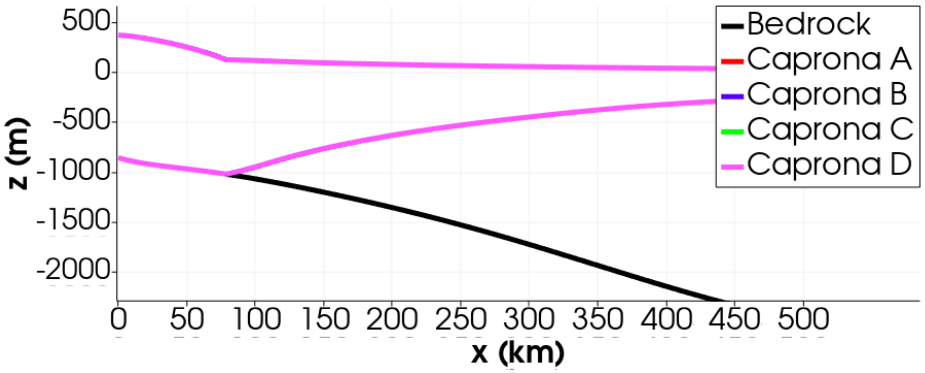

(a) Ice thickness along each Caprona profiles.

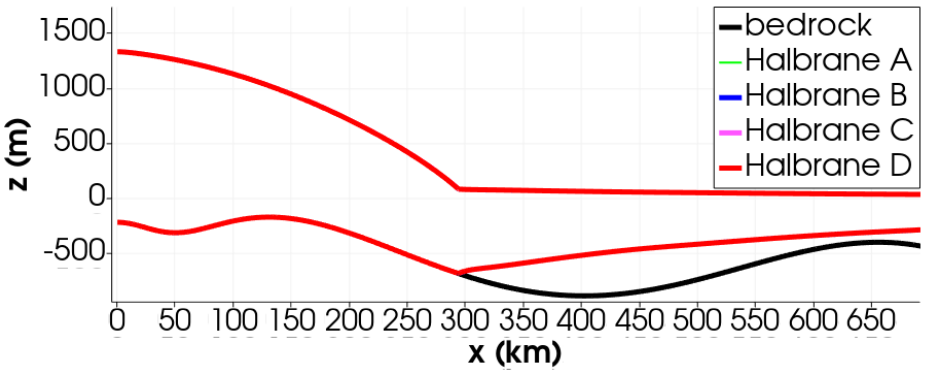

(b) Ice thickness along each Halbrane profiles.

Figure: Ice thickness along the thule domain profiles.

Results: Thule domain III

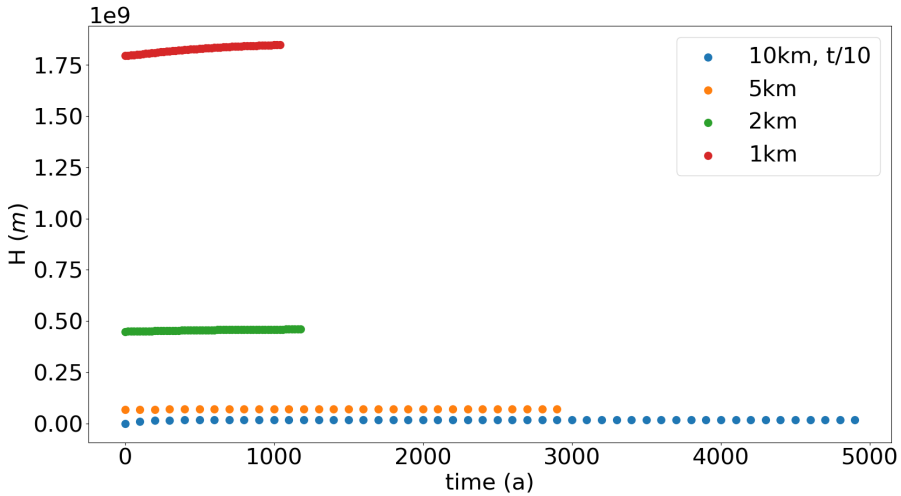

(a) Ice thickess variation in time.

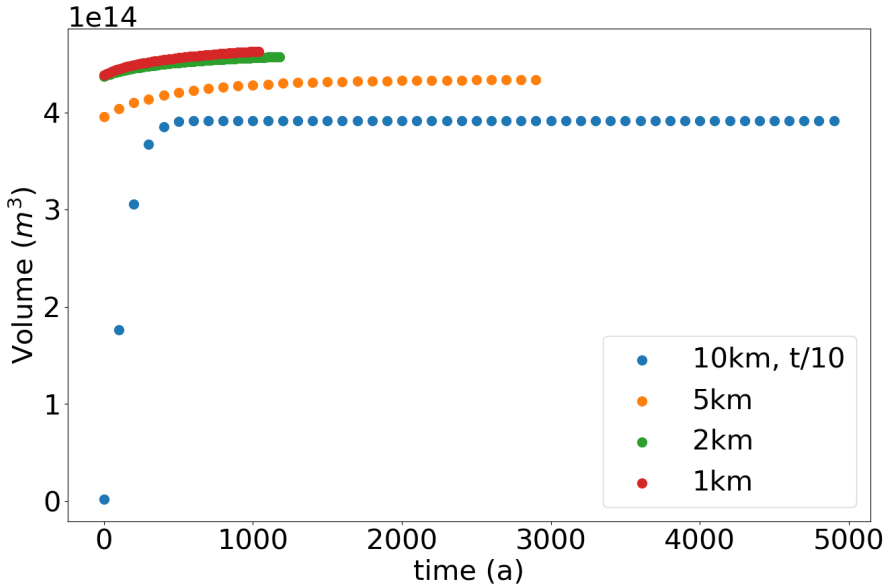

(b) Volume variation in time.

Figure: Ice thickess and volume variation in time for the Thule domain experiment.

Results: Thule domain IV

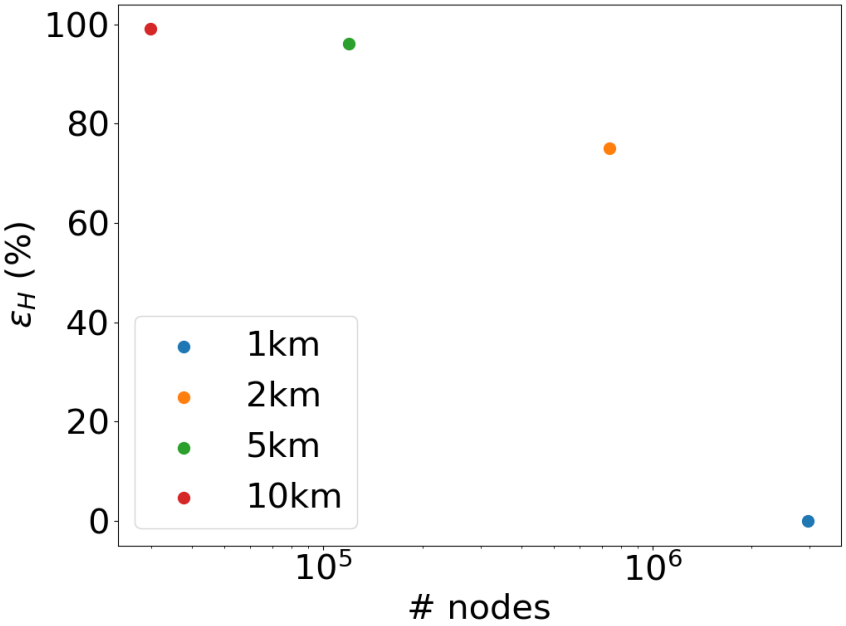

(a) Ice thickness error as a function of the number of nodes.

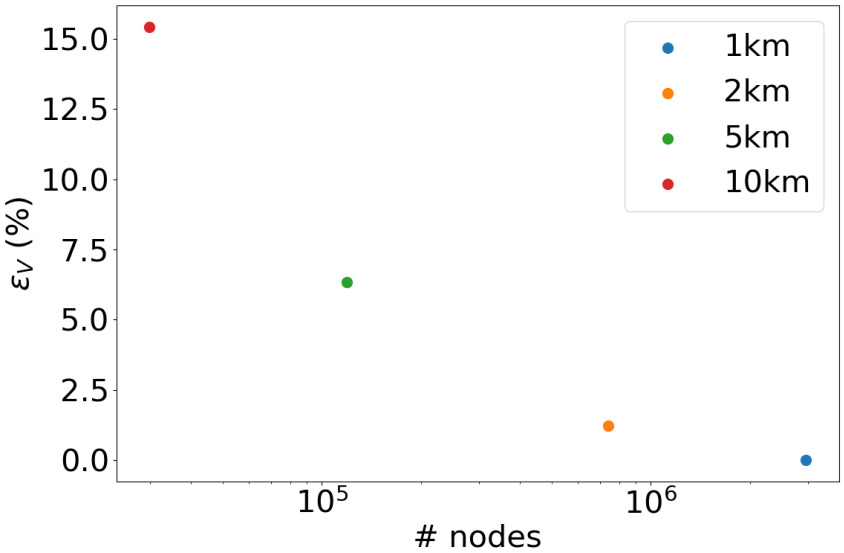

(b) Volume relative variation as a function of the number of nodes.

Figure: Volume and ice thickness variation as a function of the number of nodes for the thule domain experiment.

Results: Thule domain V

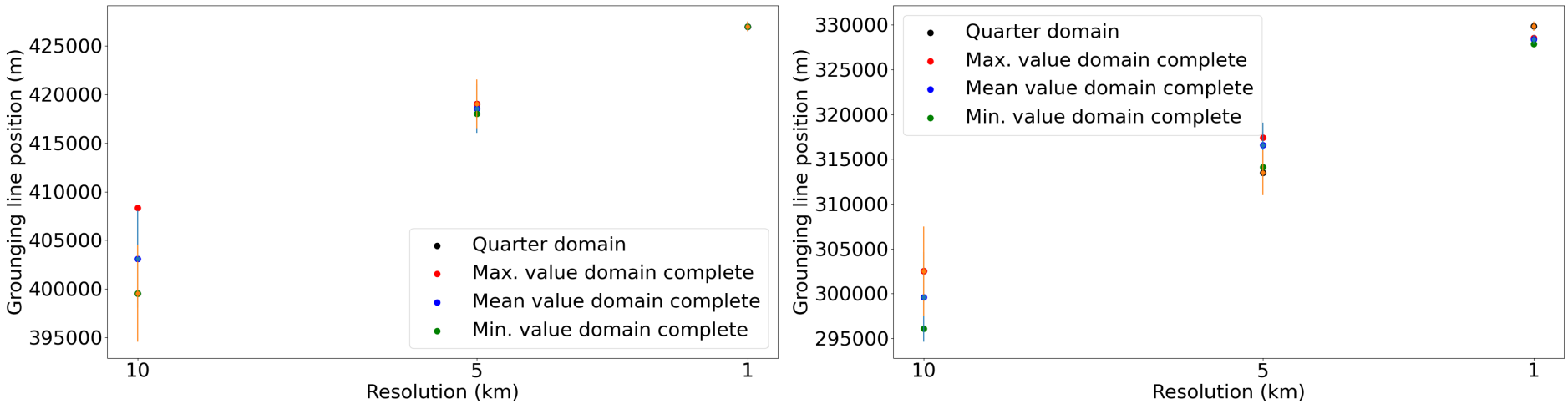

(a) Grounding line positions along Capronas profiles.

(b) Grounding line positions along Halbrane profiles

Figure: Grounding line positions as a function of the resolution for quarter and complete thule domain along the Caprona and Halbrane profiles.

Conclusions

- The results obtained for the grounding line position for both experiments were consistent with the ones carried out by Durand et al. (2009) were they could show that the grounding line position results start to be consistent for a grid size smaller than 5km.
- The grounding line position is increasing as a function of the resolution, due to the topography of both experiments.
- The fact that the grounding line position increases in a higher resolution, means that the ice thickness will also increase, since the ice column at the grounding line is now larger due to the decreasing slope of the bedrock, meaning that the ice flux through the grounding line will increase.
- The resolution has a direct impact in the symmetry of the domain of study, leading to differences in results of parts of the domain if the resolution is low.

IGE
Institut des géosciences de l'environnement

Bibliography and references I

Barbier, E. B. (2015). Climate change impacts on rural poverty in low-elevation coastal zones. *Estuarine, Coastal and Shelf Science*, 165:A1–A13.

Clark, P. U., Church, J. A., Gregory, J. M., and Payne, A. J. (2015). Recent progress in understanding and projecting regional and global mean sea level change. *Current Climate Change Reports*, 1(4):224–246.

Durand, G., Gagliardini, O., Zwinger, T., Le Meur, E., and Hindmarsh, R. C. (2009). Full stokes modeling of marine ice sheets: influence of the grid size. *Annals of Glaciology*, 50(52):109–114.

Earle, S. (2015). *Physical geology*. BCcampus.

Fricker, H. A., Coleman, R., Padman, L., Scambos, T. A., Bohlander, J., and Brunt, K. M. (2009). Mapping the grounding zone of the amery ice shelf, east antarctica using insar, modis and icesat. *Antarctic Science*, 21(5):515–532.

Bibliography and references II

Glen, J. (1958). The flow law of ice: A discussion of the assumptions made in glacier theory, their experimental foundations and consequences. *IASH Publ*, 47(171):e183.

Hanna, E., Navarro, F., Pattyn, F., Domingues, C., Fettweis, X., Ivins, E., Nicholls, R., Ritz, C., Smith, B., and Tulaczyk, S. (2013). White-25 house, pl, and zwally, hj: Ice-sheet mass balance and climate change. *Nature*, 498:51–59.

Haywood, A., Dowsett, H. J., Robinson, M. M., Stoll, D. K., Dolan, A., Lunt, D., Otto-Bliesner, B., and Chandler, M. (2011). Pliocene model intercomparison project (pliomip): experimental design and boundary conditions (experiment 2). *Geoscientific Model Development*, 4(3):571–577.

Hooke, R. L. (2019). *Principles of glacier mechanics*. Cambridge university press.

Bibliography and references III

Hutter, K. (1982). A mathematical model of polythermal glaciers and ice sheets. *Geophysical & Astrophysical Fluid Dynamics*, 21(3-4):201–224.

Montgomery, M. (2007). United nations population fund: State of world population 2007: Unleashing the potential of urban growth. *Population and Development Review*, 33(3):639–641.

Morlighem, M., Williams, C. N., Rignot, E., An, L., Arndt, J. E., Bamber, J. L., Catania, G., Chauché, N., Dowdeswell, J. A., Dorschel, B., et al. (2017). Bedmachine v3: Complete bed topography and ocean bathymetry mapping of greenland from multibeam echo sounding combined with mass conservation. *Geophysical research letters*, 44(21):11–051.

Nevermann, H., Gomez, J. N. B., Fröhle, P., and Shokri, N. (2023). Land loss implications of sea level rise along the coastline of colombia under different climate change scenarios. *Climate Risk Management*, 39:100470.

Bibliography and references IV

Weertman, J. (1974). Stability of the junction of an ice sheet and an ice shelf. *Journal of Glaciology*, 13(67):3–11.